Ocean Modelling 164 (2021) 101820

Contents lists available at ScienceDirect

Ocean Modelling

journal homepage: www.elsevier.com/locate/ocemod

Improving coastal flooding predictions by switching meshes during a simulation

Ajimon Thomas [a,b,*], J.C. Dietrich [b], M. Loveland [c], A. Samii [c], C.N. Dawson [c]

[a] Aon, 200 E Randolph Street, Chicago, IL, 60601, United States of America

[b] Department of Civil, Construction, and Environmental Engineering, North Carolina State University, 2501 Stinson Drive, Raleigh, NC, 27607 United States of America

[c] Oden Institute for Computational Engineering and Sciences, The University of Texas at Austin, Austin, TX 78712, United States of America

ARTICLE INFO

Keywords:
ADCIRC
Inundation
Hindcasting
Forecasting
Unstructured mesh

ABSTRACT

Storm surge and coastal flooding predictions can require high resolution of critical flow pathways and barriers, typically with simulations using grids/meshes with millions of cells/elements to represent a coastal region. However, the cost of this resolution can slow forecasts during a storm. To add resolution when and where it is needed, previous studies have used adaptive mesh methods, which update resolution at single or multiple cells but which require hierarchies of and thresholds for refinement, and nesting methods, which update resolution at subdomains but which require additional simulations. This research proposes a middle way, in which predictions from a coarse mesh are mapped, mid-simulation, onto a fine mesh with increased resolution near the storm's projected landfall location. The coarse and fine meshes are pre-developed, thus removing any refinement decisions during the simulation, the solution mapping uses a widely used framework, thus enabling an efficient interpolation, and the same simulation is continued, thus eliminating a separate full-domain simulation. For four historical storms, results show efficiency gains of up to 53 percent, with minimal accuracy losses relative to a static simulation.

1. Introduction

During tropical cyclones and other coastal storms, the greatest threat is storm surge, the rise of water above the normal astronomical tide. In coastal regions with relatively flat floodplains, storm surge may lead to intrusion of ocean waters 10 to 20 miles inland (Conner et al., 1957), with devastating effects to infrastructure and ecosystems. Storm-driven coastal flooding can be predicted with numerical models, which must represent physical processes and geographical features that influence storm surge from the deeper ocean, onto the continental shelf, into estuaries and marshes, and over low-lying coastal floodplains. These multi-scale processes led to the development of models that can increase resolution of coastal features. However, there is a continuing challenge to provide high resolution only when and where it is required, with the goal of optimizing the efficiency of simulations, especially in forecasting applications when model predictions are required to support decision-making (Cheung et al., 2003).

Storm surge and coastal flooding can be predicted with the ADvanced CIRCulation (ADCIRC) modeling system (Luettich and Westerink, 2004; Westerink et al., 2008), which is used for long-term planning and design (U.S. Army Corps of Engineers, 2018; FEMA, 2021), evaluation of surge mitigation systems (Interagency Performance Evaluation Task Force, 2008), and operational forecasting (National Oceanic, Atmospheric Administration, 2021). ADCIRC uses unstructured, finite-element meshes in which resolution can vary over 3 to 4 orders of magnitude (Hope et al., 2013; Roberts et al., 2019). These meshes can be large in their spatial coverage, with millions of finite elements to represent one or multiple state coastlines (Thomas et al., 2019), and in their cost, requiring several hours even on thousands of computational cores (Dietrich et al., 2012). A significant portion of the cost is due to the inclusion of floodplains and other sub-aerial regions, which remain dry for most of the simulation and become wet only as the storm makes landfall, but which are represented typically by 50 to 90 percent of the total number of finite elements (Roberts et al., 2021). Although ADCIRC meshes can be designed to reduce the number of elements in these floodplains (Bilskie et al., 2020), there is a need to adapt during the simulation to include the floodplains only as they are wetted.

One possibility is adaptive mesh methods, in which meshes are refined dynamically to obtain fine-scale solutions in areas of interest, e.g. to follow a tsunami or near landfall of a coastal storm (Berger et al., 2011; Mandli and Dawson, 2014; Caviedes-Voulliéme et al., 2020).

* Corresponding author at: Department of Civil, Construction, and Environmental Engineering, North Carolina State University, 2501 Stinson Drive, Raleigh, NC, 27607 United States of America.
E-mail addresses: athomas9@ncsu.edu (A. Thomas), jcdietrich@ncsu.edu (J.C. Dietrich).

https://doi.org/10.1016/j.ocemod.2021.101820
Received 17 October 2020; Received in revised form 8 April 2021; Accepted 30 May 2021
Available online 2 June 2021

Elements are split or joined, either individually or in patches, based on gradients in topography or hydrodynamics, and thus these methods require a hierarchy of information at varying levels of resolution, as well as decisions about how and when to refine or coarsen across that hierarchy (Kubatko et al., 2006; Gerhard et al., 2015). For structured meshes, these methods must overcome the challenges of conservation and well-balancing, gradation of element sizes, and selection of refinement thresholds (Liang and Marche, 2009; Berger et al., 2011; Kesserwani and Liang, 2012; Liang et al., 2015; Hou et al., 2018), as well as spurious momentum and smaller time steps (Caviedes-Voulliéme et al., 2020). For unstructured meshes with triangular elements, the methods must also address the challenges of unintentional generation of skewed triangular elements (Behrens et al., 2005) and the structured design of hierarchies for efficient refinement (Behrens and Bader, 2009). Recent studies have demonstrated successful applications for urban flooding (Hu et al., 2018) and idealized storms and domains (Beisiegel et al., 2020), with speed-ups of 70 percent relative to models with static meshes. However, due partly to the challenges listed above, adaptive mesh methods have not yet been applied for realistic storm surge simulations using unstructured meshes.

Another possible adaptive technique is nesting, in which a simulation with a fine-resolution mesh is forced with results from a separate simulation with a coarser mesh, e.g. for the investigation of tropical cyclones and mid-latitude disturbances and in coastal ocean applications (Ookochi, 1972; Mathur, 1974; Hovermale, 1976; Miyakoda and Rosati, 1977; Oey and Chen, 1992). For structured meshes, nesting has been implemented in one or two directions (ways), depending on whether information from the fine-scale simulation is sent back to the large-domain simulation. Two-way nesting has been applied extensively, such as in ROMS AGRIF (Penven et al., 2006; Debreu et al., 2008, 2012), including for storm surge hindcasts (Pianezze et al., 2020) and forecasts (Dinapoli et al., 2020). For unstructured meshes, a one-way nesting was tested for two small estuarine systems using an outer large-scale coarse mesh and an inner small-scale fine mesh (Taeb and Weaver, 2019), with run-time reductions of 54% to more than 80%, and with the solutions showing relatively small deviations from the conventional single-domain technique. Also with unstructured meshes, a related technique is subdomain modeling (Baugh et al., 2015; Altuntas and Baugh, 2017), in which a single full-domain simulation is used as forcing to repeated simulations on subdomains with local changes, e.g. possible configurations of ground surface and hydraulic barriers to consider design alternatives for a coastal structure. These techniques are similar in that they use coarse-scale information as forcing to predictions at finer resolution. However, because the coarse simulation must be performed before or alongside the fine simulation, it can increase costs in operations.

We propose a multi-resolution approach to share the advantages of both the adaptive mesh methods and nesting techniques. Our approach is adaptive in that resolution is increased during the simulation, but it does not require a hierarchical mesh refinement. And our approach is nested in that results are mapped onto a pre-developed, higher-resolution mesh for the same coastal region, but it does not require boundary conditions from a separate full simulation. The simulation will start with a mesh without extensive coastal detail while the storm is far away, its results will be mapped onto an available mesh with better representation of the coastal region to be affected by the storm, and then the simulation will continue with higher-resolution predictions of coastal flooding as the storm makes landfall. *We hypothesize that, by 'switching' during a simulation from coarse- to fine-resolution meshes, with the resolution in the fine mesh concentrated only at specific coastal regions influenced by the storm, both accuracy and computational gains can be achieved.* The multi-resolution approach is implemented into ADCIRC for use on its unstructured meshes. This approach is most promising for real-time forecast applications. In the following sections, we describe the mechanics of the multi-resolution approach and then demonstrate gains in accuracy and efficiency for representative storms.

2. Methods

2.1. Ocean circulation models and technologies

ADCIRC will be used for simulations of storms along the U.S. southeast and Texas coasts, starting on a coarse mesh. During each simulation, a new technology called *Adcirpolate* will allow for regridding of the computed solution from coarse to fine meshes. Then each simulation will continue on a fine mesh.

2.1.1. ADCIRC

To predict coastal flooding, we use the ADvanced CIRCulation (ADCIRC) modeling system, which has been validated extensively for storms around the world (Bhaskaran et al., 2013; Hope et al., 2013; Suh et al., 2015; Dietrich et al., 2018). ADCIRC (Luettich et al., 1992; Luettich and Westerink, 2004; Westerink et al., 2008) is a depth-integrated, shallow-water, finite-element model capable of simulating tidal circulation and storm-surge propagation over large computational domains. ADCIRC is used by the Federal Emergency Management Agency (FEMA) in the development of flood insurance rate maps (Federal Emergency Management Agency, 2019), by the U.S. Army Corps of Engineers (USACE) for navigation and storm protection projects (U.S. Army Corps of Engineers, 2018), and also by the National Oceanic and Atmospheric Administration (NOAA) for tidal calibrations and incorporation into its vertical datum transformation software VDatum (Myers et al., 2007). In this study, the depth-averaged, barotropic version of ADCIRC is used because the strong surface stresses during storms cause the water column to be well-mixed in shallow nearshore and coastal regions. This study will ignore storm-induced wave effects, i.e. no coupling with a nearshore wave model.

For the simulations in this study, the ADCIRC version 54.dev is used in explicit mode with the lumped mass matrix form of the Generalized Wave Continuity Equation (GWCE) (Tanaka et al., 2011). A depth-dependent quadratic friction law is used to apply bottom drag, with the drag coefficient as computed from Manning's n values (Luettich et al., 1992; Luettich and Westerink, 2004). The air–sea momentum exchange is parameterized as a wind drag (Garratt, 1977) with an upper limit of $C_D = 0.002$, similar to other studies (Dietrich et al., 2011, 2012). Spatially varying attributes are used to represent Manning's n values, eddy viscosity, the primitive weighting in the GWCE, surface roughness, surface canopy, elemental slope limiter, and advection; many of these attributes are derived from land cover data. A spatially-varying offset-surface was also used to account for water level processes on longer time scales like steric and local sea level rise (Thomas et al., 2019).

2.1.2. Adcirpolate

The proposed multi-resolution approach uses a technology called *Adcirpolate* (Samii, 2021) to switch simulations between pre-developed coarse and fine meshes. When a storm is in the open ocean, there is uncertainty where it will make landfall. At this time, a simulation can be started with a mesh with an extensive coverage of the U.S. coastline but having a relatively coarse resolution of coastal features. As the storm approaches the coastline and the landfall location becomes more certain, the computed solution is switched to a fine-resolution mesh that describes the coastal features in that region in high detail. The initiation of the switch is decided by the modeler; example criteria for and costs of switching are quantified later in this study.

The switching technology is implemented via the Earth System Modeling Framework (ESMF, Hill et al. (2004)) and operates on the ADCIRC hot-start files (named `fort.67` or `fort.68` in the ADCIRC convention), which include solution fields for surface elevations, depth-averaged velocities, wet/dry states, etc. at previous and current time steps. Using the ESMF routines, the fine/destination mesh is masked to identify regions within the coverage of the coarse/source mesh (e.g. along the open coast) and regions outside the coverage of the coarse/source mesh (e.g. inland floodplains). Then the fields from the

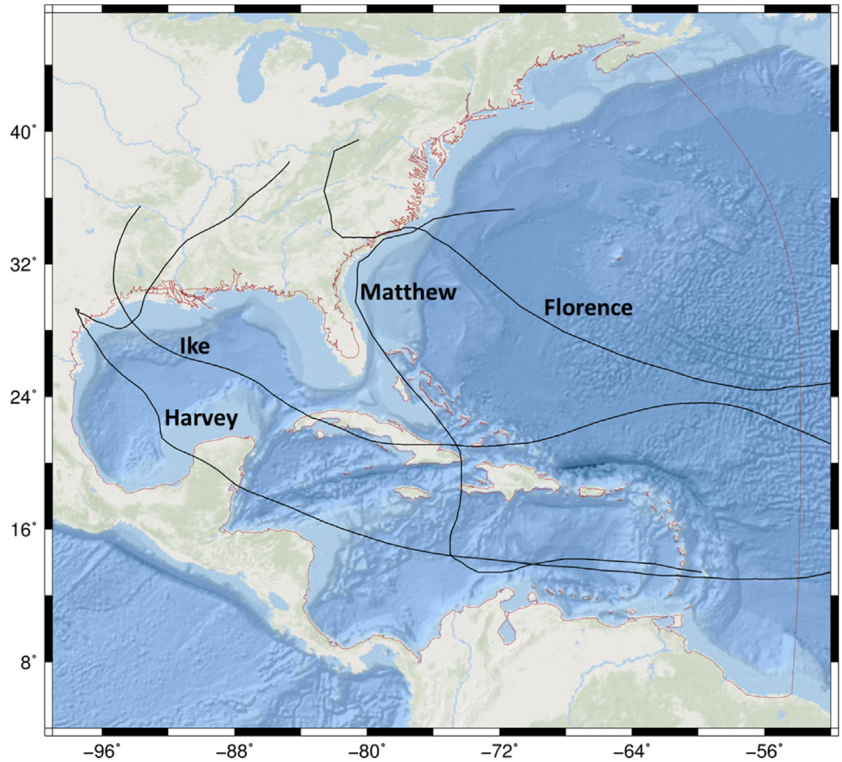

Fig. 1. Storm tracks (from best tracks reported by the National Hurricane Center) for Ike, Matthew, Harvey, and Florence. The HSOFS mesh boundary is shown in brown.

coarse/source mesh are regridded onto the fine/destination mesh. For points within the coverage, the solution fields are regridded by using bilinear interpolation. For points outside the coverage, the solution fields are regridded by extrapolation with nearest source to destination, i.e. each destination point is mapped from the closest source point, and a source point can be mapped to multiple destination points. The regridding is done in parallel and on an arbitrary number of CPUs, i.e. it is not confined to the number of cores from either the coarse or fine simulations. The resulting hot-start file is then used to continue the simulation on the fine mesh.

The regridding is demonstrated in an example application in the Appendix. Here, we note that *Adcirpolate* is not conservative globally or locally. The intention is for the fine mesh to include inland water bodies (bays, estuaries, natural and man-made channels) that are not represented in the coarse mesh, and thus the regridding cannot conserve mass and momentum in a global, domain-wide sense. However, even for a local, single-element sense, the regridding will not be conservative. For instance, a channel may be artificially wide in the coarse mesh (due to large element sizes) but represented at its correct width in the fine mesh, or a nearshore bathymetry may be artificially smoothed in the coarse mesh but represented with its submerged ridges and channels in the fine mesh. However, as we demonstrate in this study, the nonconservative mapping does not prevent the follow-on simulation from providing accurate predictions of storm surge and coastal flooding.

2.1.3. *Unstructured meshes*

ADCIRC uses unstructured, finite-element meshes to describe the coastal ocean. For storm simulations in this study, we will start on a coarse mesh (called HSOFS) with coverage of the entire U.S. coast, and then switch to a fine mesh for the coast along either the South Atlantic Bight (SAB) or Texas.

The coarse mesh will be required for simulations for daily, non-storm conditions, as well as for storms as they develop far from shore. This study uses the well-validated Hurricane Surge On-Demand Forecasting System (HSOFS) as the coarse mesh due to its extensive coverage of nearshore regions and coastal floodplains along the U.S. coast from Texas through Maine (Riverside Technology, AECOM, 2015). The HSOFS mesh has an average resolution of 500 m along the coast with some areas decreasing to 150 m. At most locations, the mesh extends inland to the 10-m topographic contour. It has 1,813,443 vertices and 3,564,104 elements. For ADCIRC simulations on the HSOFS mesh, the spatially constant horizontal eddy viscosity for the momentum equations was set to 50 m^2 s^{-1}, a time step of 1 s was used, and the advective transport terms were enabled to account for nonlinear interactions between surge and tides.

For storms affecting the coast along the South Atlantic Bight (SAB), we will switch from HSOFS to a new SAB mesh. This high-resolution mesh has detailed coverage from Florida through North Carolina and was developed by merging five FEMA regional meshes (Thomas, 2020). The SAB mesh has 5,584,241 vertices and 11,066,018 elements. Its resolution increases to 100 m along the southeastern U.S. coastline, except in a few regions along the Carolina coasts. The resolution is 10 m in some channels in Florida. For ADCIRC simulations on the SAB mesh, a set of spatially variable parameters was developed using the attributes of the FEMA regional meshes. The advective transport terms were enabled. However, the SAB mesh, owing to its high resolution, requires a smaller time step of 0.5 s to satisfy the Courant–Friedrichs–Lewy (CFL) condition that relates the model time step, element size and wave speed (Luettich et al., 1992).

For storms affecting the western Gulf of Mexico, we will switch from HSOFS to the so-called Texas mesh, which is well-validated for storm surge predictions along the Texas coast (Kennedy et al., 2011; Sebastian et al., 2014). It has 3,331,560 vertices and 6,633,623 elements. The resolution along the Texas coastline is approximately 100 m, with increased resolution to 30 m to represent the complexity around the Galveston area. For ADCIRC simulations on the Texas mesh, the time step is 1 s, but the advective transport terms are disabled to improve numerical stability.

2.2. *Storms and atmospheric forcing*

The proposed approach is evaluated with four storms: Ike (2008), Matthew (2016), Harvey (2017), and Florence (2018) (Fig. 1). These

Table 1
Start and end date/times for the storm simulations. For each storm, the *Coarse* and *Fine* simulations used the full 9-day storm duration on their respective meshes, whereas the *Mixed* simulations were started on the coarse mesh and then switched onto a fine mesh. The date/time for each switch was determined from hydrographs at coastal stations; when the water levels increased above the normal tide range, then the simulation was switched onto the fine mesh.

Storm	Year	Start	Days	Switch	Days	End
Ike	2008	1200 UTC 05 Sep	6	1200 UTC 11 Sep	3	1200 UTC 14 Sep
Matthew	2016	0000 UTC 02 Oct	4.5	1200 UTC 06 Oct	4.5	0000 UTC 11 Oct
Harvey	2017	0000 UTC 22 Aug	3	0000 UTC 25 Aug	6	0000 UTC 31 Aug
Florence	2018	0000 UTC 07 Sep	6	0000 UTC 13 Sep	3	0000 UTC 16 Sep

storms are hindcasted by using data-assimilated products from Oceanweather Inc. as forcing to ADCIRC simulations.

2.2.1. Historical storms

Ike was a Category-4 hurricane (on the Saffir–Simpson wind scale), made landfall along the upper Texas coast with Category-2 intensity during September 2008 (Berg, 2009), and pushed surge as high as 4.5 to 6 m on the Bolivar Peninsula and in parts of Texas. Matthew was a Category-5 hurricane that caused widespread impacts all along the U.S. southeast coast, and made landfall with Category-1 intensity along the central coast of South Carolina during October 2016 (Stewart, 2017). Harvey was a Category-4 hurricane that made landfall at peak intensity in middle Texas coast, stalled over southern Texas for days, and resulted in catastrophic flash and river flooding. Florence was a Category-4 hurricane that made landfall along the southeastern coast of North Carolina during September 2018 (Stewart and Berg, 2019), and caused significant storm surge flooding in eastern North Carolina.

These storms were selected because of their varied landfall locations, tracks, and other parameters. Matthew and Florence affected the Atlantic coast, whereas Ike and Harvey affected the Texas coast. Matthew's track was shore-parallel from Florida to North Carolina, Harvey's track started as shore-normal but became shore-parallel as it stalled over Texas, and Ike's and Florence's tracks were shore-normal. They also had variations in parameters including track orientation to shoreline, intensity of winds, duration, size, etc. The proposed approach will be tested in these four cases to demonstrate its capability for any storm.

2.2.2. Atmospheric forcing

This study will consider hindcasts of the four storms by using data-assimilated surface pressure and wind velocities from Oceanweather Inc. (OWI). These atmospheric products are based on observations from anemometers, airborne and land-based Doppler radar, airborne stepped-frequency microwave radiometer, buoys, ships, aircraft, coastal stations and satellite measurements (Bunya et al., 2010). In-situ data sources can be inaccurate at hurricane wind speeds (Cardone and Cox, 2009) and also inadequate to resolve the evolution of the critical inner core structure. Indirect methods using a variety of models are therefore used to describe the evolution of the hurricane wind fields. These include simple parametric models (Holland, 1980), steady-state dynamical models like the Planetary Boundary Layer (PBL) model (Fauver, 1970; Vickery et al., 2000), non-steady dynamical methods like NOAA's WRF model (Corbosiero et al., 2007), and kinematic methods like the NOAA Hurricane Research Wind Analysis System (H*WIND) (Powell et al., 1996, 2010). These methods can also be combined by blending an inner core wind field to a peripheral large-scale wind field using the Interactive Object Kinematic Analysis (IOKA) system (Cox et al., 1995; Cardone and Cox, 2009). These fields have been used in ADCIRC hindcasts of Katrina (Dietrich et al., 2010), Ike (Hope et al., 2013; Kennedy et al., 2011), Gustav (Dietrich et al., 2011), and other storms. Compared to parametric vortex models like the Generalized Asymmetric Holland Model (GAHM) (Gao et al., 2017) used during forecasting, OWI fields have been shown to be the most realistic representation of the atmospheric forcing during storms (Thomas et al., 2019).

Depending on the storm, the OWI fields can be presented with a lower-resolution, basin-wide grid and nested, higher-resolution, regional grids. For Ike, the basin grid covers from 17.93°N to 30.73°N and from 98.03°W to 60.03°W with a spatial resolution of 0.1°, whereas the higher-resolution region field covers from 28.43°N to 30.185°N and from 96.03°W to 93.03°W with a spatial resolution of 0.015°, both covering a period from 1200 UTC 05 September 2008 until 0600 UTC 14 September 2008, at 15 min intervals. For Matthew, the basin grid covers from 5°N to 47°N and from 99°W to 55°W with a spatial resolution of 0.25°, whereas the higher-resolution region field covers from 15°N to 40°N and from 82°W to 68°W with a spatial resolution of 0.05°, both covering a period from 0000 UTC 01 October 2016 until 0000 UTC 11 October 2016, at 15 min intervals. For Harvey, the basin grid covers from 5°N to 47°N and from 99°W to 55°W with a spatial resolution of 0.25°, whereas the higher-resolution region field covers from 18°N to 30.96°N and from 98°W to 80°W with a spatial resolution of 0.08°, both covering a period from 1200 UTC 13 August 2017 until 0000 UTC 15 September 2017, at 15 min intervals. For Florence, the basin grid covers from 5°N to 47°N and from 99°W to 55°W with a spatial resolution of 0.20°, whereas the higher-resolution region field covers from 31°N to 37°N and from 82°W to 74°W with a spatial resolution of 0.05°, both covering a period from 0000 UTC 07 September 2018 until 0000 UTC 18 September 2018, at 15 min intervals. For all storms, the surface wind and pressure fields are interpolated in time and space onto the ADCIRC unstructured meshes.

2.3. Simulations and analyses

For each storm, we consider three simulations: *Coarse*, *Mixed*, and *Fine*. For the *Mixed* simulations to be beneficial, we must identify a parameter to switch late enough to optimize efficiency on the coarse mesh, but early enough to optimize accuracy on the fine mesh. These optimizations will be evaluated by comparing the computed solutions and via wall-clock times.

2.3.1. Switching parameters

For the *Coarse* simulations, the HSOFS mesh is used for the entire storm, and for the *Fine* simulations, either the SAB or Texas mesh is used for the entire storm. For the *Mixed* simulations, the HSOFS mesh is used when the storm is away from a coastline and its path is uncertain, but then we switch to the fine mesh for that region as the storm starts to affect water levels along the coast. The switching times for the *Mixed* simulations were determined from observed time series of water levels. The idea is to identify the time at which the total water levels become influenced by the storm (Thomas, 2020). An ideal switching time will result in near-zero differences in water levels overall (and thus a minimal loss in accuracy), while occurring as late as possible during the storm (and thus a maximum gain in efficiency). The simulation durations and the switching times for the *Mixed* simulations for all four storms are shown in Table 1.

For Ike, switching was done when the eye of the storm was located about 500 km south of Dauphin Island, AL. At this time, the water levels along the TX coastline were 0.70 m at the entrance of Galveston Bay, 0.70 m at Corpus Christi, and 0.54 m at Port Isabel. For Matthew, switching was done when the storm was located 500 km south of Nassau, Bahamas when the water levels were 0.01 m at Vaca Key, −0.11 m at Virginia Key, and −0.10 m at Lake Worth Pier, FL. For Harvey, switching was done when the storm was located 500 km south of Galveston Bay, TX. Water levels at various points along the TX coastline were 0.40 m at Sabine Pass, 0.54 m at the entrance to the

Galveston Bay, 0.39 m at Corpus Christi, and 0.32 m at Port Isabel. For Florence, switching was done when about the storm-eye was located about 477 km off the Hatteras Inlet, NC. The water levels at this time were 0.46 m at Wrightsville Beach, 0.26 m at Beaufort, and 0.25 m at Hatteras.

2.3.2. Error statistics

The agreement between observations and predicted results is quantified by using error metrics of root-mean-squared error (E_{RMS}) and mean normalized bias (B_{MN}) (Thomas et al., 2019). The E_{RMS} indicates magnitude of the error and has an ideal value of zero, whereas the B_{MN} is a measure of the model's over- or under-prediction normalized to the observed value, and also has an ideal value of zero. A positive B_{MN} indicates over-prediction, while a negative value indicates under-prediction by the model. The predicted and observed peak water levels are also analyzed with the coefficient of determination (R^2) and best-fit slope (m). The R^2 is a statistical measure of how close the data is to the linear regression model, and has an ideal value of unity. The best-fit slope is the slope of the line that best represents the relationship between observed and predicted data, and also has an ideal value of unity.

The accuracy of the approach is also evaluated by comparing the total volume of inundation to that from the *Coarse* and *Fine* simulations. For an element, this volume is equal to the area of the element multiplied by the average depth of water (height of water above the ground surface) in the three vertices. An element contributes to the total volume only if all the three vertices: (1) have ground surface elevations above mean sea level, (2) are located in the affected area of the storm, and (3) were flooded during the simulation. It is noted that, because the ground surface is represented at differing resolutions in these simulations, the volume of inundation will be affected by the resolution.

The efficiency of the approach is evaluated by comparing the wall-clock time of simulations with and without switching. All simulations were completed on the Stampede2 computing cluster at the Texas Advanced Computing Center, using 522 computational cores. For the approach, a total of the times required for the coarse part of the simulation, *Adcirpolate*, and the fine part is taken for comparison. To avoid any inconsistencies with run-times due to hardware, competing jobs, or network traffic, each simulation is run three times on the same number of cores, and the minimum of the three run-times is then used for comparisons. However, in operations, there is no restriction on the numbers of cores used for the coarse or fine simulations or *Adcirpolate*.

3. Results and discussion

In this study, we hindcast four storms, each having different parameters like track, intensity, flooding extent, etc. For each storm, we perform three simulations: *Coarse*, *Fine*, and *Mixed*. The results from these simulations are then analyzed to quantify the benefits of the proposed approach.

3.1. Accuracy benefits

3.1.1. Comparisons of predicted flooding extents

To examine the effects of higher resolution on predictions of overland flooding, difference maps of maximum water levels between the *Coarse*, *Mixed*, and *Fine* simulations are plotted for all four storms (Fig. 2). Differences are shown at the fine-mesh resolution by mapping the *Coarse* and *Mixed* results to the fine mesh. Overall, there are significant differences between the *Coarse* and *Fine* maximum water levels for all four storms, and these are attributed to the difference in mesh geometry between the coarse and fine meshes. For Matthew and Florence, these differences mainly occur inland, with near-zero differences nearshore and in the open ocean. For Ike and Harvey, larger differences are both nearshore and inland, with larger magnitude near the landfall location. For Ike, the *Fine* maximum water levels exceeded the *Coarse* results by as much as 1.25 m in the rivers, bays and lakes located north of Galveston Bay, Texas. These large differences were likely due to how the bottom friction is parameterized on the Louisiana-Texas meshes in both meshes, with the Texas mesh using a lower friction that enabled predictions of the Ike forerunner (Kennedy et al., 2011).

For all storms, the *Mixed* and *Fine* maximum water levels were a good match, as evident from the near-zero differences in the open-ocean, nearshore and inland regions. Differences in the open-ocean and nearshore regions were small (less than 0.15 m) and related to the time of switching in the *Mixed* simulation, and differences in inland regions are due to the difference in geometry between the coarse and fine meshes.

Harvey produced maximum inundation levels of 2.5 to 3 m to the north and east of its two landfalls in Texas, in the backbays between Port Aransas and Matagorda, including the Copano Bay and Lavacaa Bay, Texas (Fig. 2, third row, left column). Compared to the *Coarse* results, the *Fine* maximum water levels are higher along the coast and inland. Along the coast, these differences are small, in the range of 0.1 to 0.2 m. The differences inland were 0.15 m in Corpus Christi Bay, 0.2 m in San Antonio Bay, 0.35 m in Matagorda Bay, and 0.35 to 0.9 m in Lavaca Bay. These differences are mainly related to the difference in the ground surface representation between the Texas mesh and the HSOFS mesh. The *Mixed* results are a good match to the *Fine* results, as evident from the zero differences along the Texas coastline. The lone exception is a location south of Baffin Bay, away from the landfall location (Fig. 2, third row, right column), where the *Mixed* maximum water levels are higher than the corresponding *Fine* values by more than 30 cm. These differences are caused by differences in how the ground surface is represented between the HSOFS and Texas meshes, and thus independent of the switching process.

For Florence, as compared to the *Coarse* results, the *Fine* water levels are higher in regions like the Albemarle Sound, Atlantic Intracoastal Waterway, Core Sound, Currituck Sound and upstream all major rivers (Fig. 2, last row, middle column). These differences were 0.1 to 0.2 m in the Core Sound, 0.2 to 0.6 m upstream of the Neuse River, 0.1 to 0.2 m in the Currituck Sound, and 0.2 to 1 m up-stream of the Pamlico River. This is attributed to the higher resolution in the fine mesh that better represents bathymetry, and in turn, a better hydraulic connectivity for water to flow into these complex regions. In the coarse mesh, the water is not able to flow into the rivers and instead is stuck at downstream locations. Downstream of the Neuse River, the *Coarse* water levels were higher by as much as 0.35 m. There are almost zero differences in the open ocean, along the coast, and in the Pamlico Sound. The differences between the *Mixed* and *Fine* results are almost-zero (Fig. 2, last row, right column), as switching has happened well before the storm impacted the NC coast. Small differences exist in the northeast region of the domain far away from the storm's impact. These differences are contributed by the coarse part of the *Mixed* simulation due to the large difference in resolution between the coarse and fine meshes.

3.1.2. Localized benefits

It is expected that the fine-mesh resolution will have its largest benefits at inland locations, because it will better represent the connectivity of storm surge from the open coast and through the rivers and other channels. Predicted water levels are compared at inland locations during Matthew and Ike, to highlight the benefits of the approach in matching *Fine* results even at locations far from the coastline. For Matthew, water levels are compared at 3 stations along the Savannah River on the GA-SC border (Fig. 3). Stations 1 and 2 are located upriver, where the resolution is insufficient in the coarse mesh, as shown by the poor simulation of the tidal signal at these locations before the switch. But after the switch, the *Mixed* and *Fine* results match well. At Station 3 closer to the open coast, both meshes have sufficient resolution of the

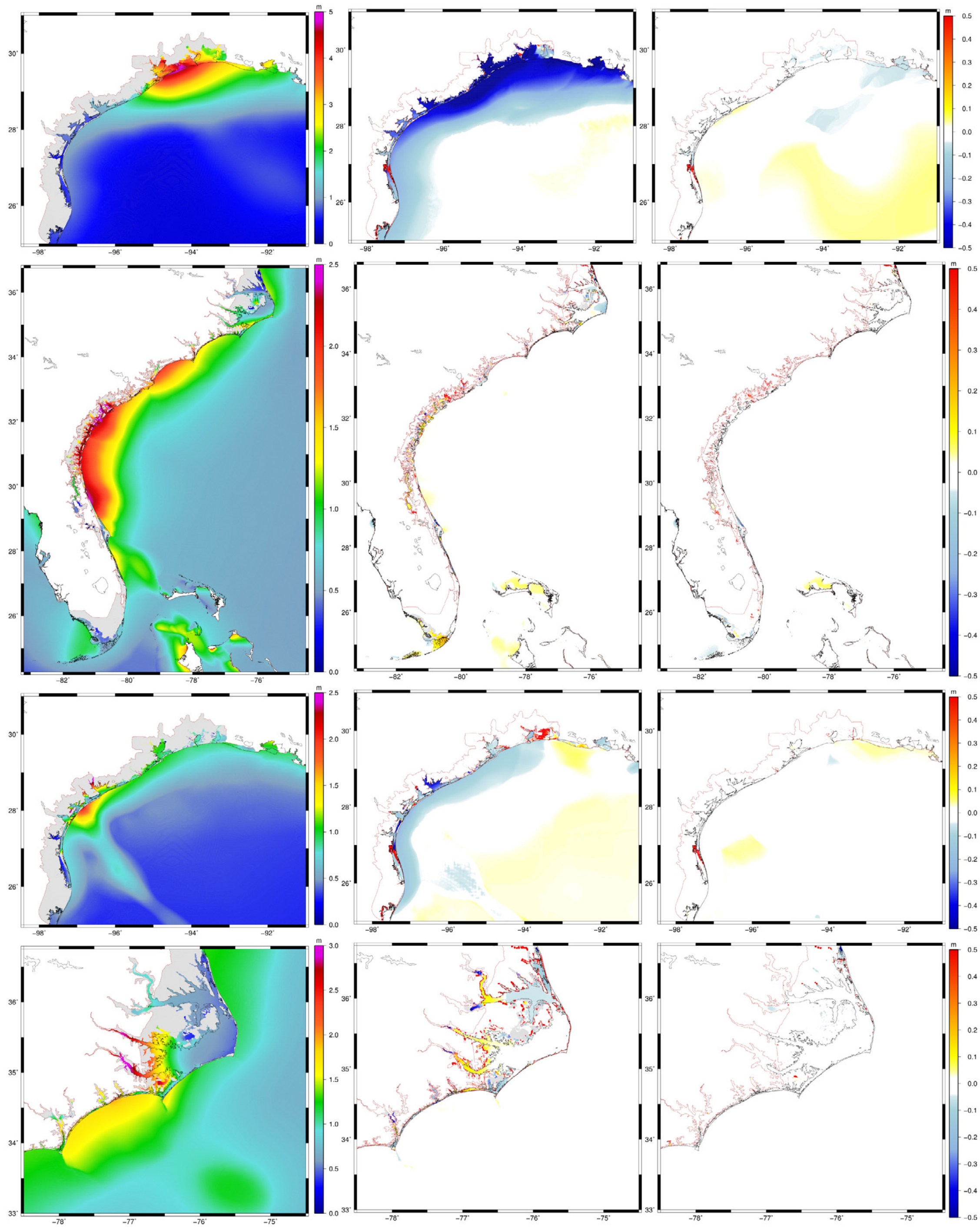

Fig. 2. Difference in maximum water levels between the *Coarse*, *Mixed*, and *Fine* simulations. Columns correspond to: (left) *Fine* maximum water levels (m relative to NAVD88), (center) difference between *Coarse* and *Fine* maximum water levels, and (right) difference between *Mixed* and *Fine* maximum water levels. Rows correspond to: (top) Ike, (second from top) Matthew, (second from bottom) Harvey, and (bottom) Florence. The coastline is shown in black and the fine-mesh boundary in brown.

storm surge at this location, and hence the *Coarse* and *Mixed* results are a good match before and after the switch.

A similar analysis is made at three stations located north of the Trinity and Galveston Bays in Texas during Ike (Fig. 4). Stations 1 and 2 are located where the coarse mesh does not possess sufficient resolution to represent the San Jacinto River. Therefore, the coarse part of the *Mixed* results stays dry. But after the switch, the *Mixed* water levels match well to the *Fine* results. At station 3, the coarse mesh has sufficient resolution to represent the storm surge, but the results are slightly different from the *Fine* simulation as the fine mesh has a much higher resolution and thus it predicts flooding better. At all three locations, the *Mixed* results match the *Fine* results after the switch. Thus the approach improves predictions of water levels at inland stations where the fine mesh has a better representation of the flow pathways.

3.1.3. Quantifying accuracy

The accuracy of the *Coarse* and *Mixed* results are analyzed by comparing them to the *Fine* solution, which is taken as the 'truth' (Table 2). This allows for an evaluation of accuracy throughout the entire region, not only where observations were collected. For this comparison, the *Coarse* results are mapped onto the fine mesh as a post-processing step, so comparisons can be made at the same resolution. For

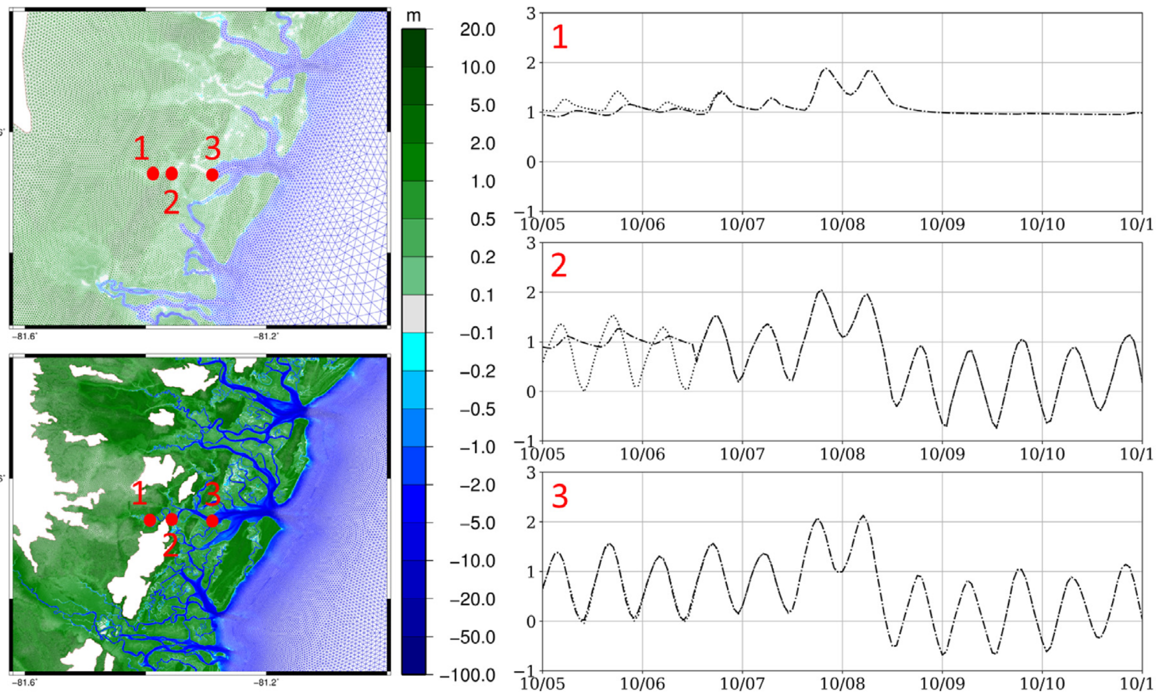

Fig. 3. Effect of mesh resolution on flooding predictions at inland stations during Matthew. Columns correspond to: (left) bathymetry and topography in the coarse (upper) and fine (bottom) meshes at a section along the Savannah River; and (right) time series of water levels (m relative to NAVD88) at the 3 locations indicated by red dots, with line types corresponding to: (dashed–dotted) *Mixed*, and (dotted) *Fine*.

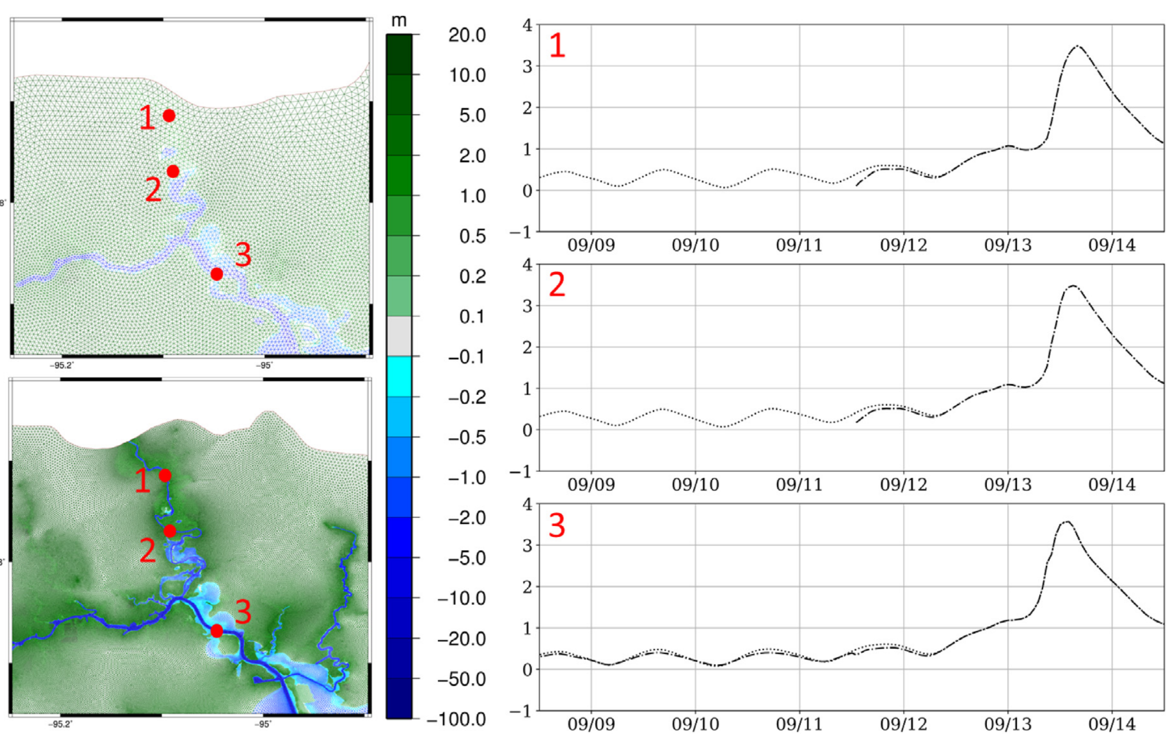

Fig. 4. Effect of mesh resolution on flooding predictions in inland stations during Ike. Columns correspond to: (left) bathymetry and topography in the coarse (upper) and fine (bottom) meshes in the San Jacinto River; and (right) time series of water levels (m relative to NAVD88) at the 3 locations indicated by red dots, with line types corresponding to: (dashed–dotted) *Mixed*, and (dotted) *Fine*.

the *Mixed* simulation, the maxima of water levels from all parts of the simulation are considered. Results are compared only at vertices in the affected area of the storm (FL to NC for Matthew, NC for Florence, TX for Harvey and Ike), that are not in open-ocean (depths less than 10 m), and that were wetted in both simulations.

For all four storms, the *Mixed* results have a B_{MN} either equal to or close to zero, whereas the *Coarse* results have a negative value indicating an overall under-prediction by the model. The *Mixed* results also have a best-fit line slope equal to or close to unity, indicating a good match to the *Fine* results. The E_{RMS} (closer to zero) and R^2

Table 2
Accuracy error metrics for the *Coarse* and *Mixed* flooding predictions for all four storms. The results were mapped onto the fine mesh, and then the error metrics were computed relative to the *Fine* flooding predictions. Stations were fine-mesh vertices that (1) had bathymetric depths less than 10 m, (2) were located in the affected area of the storm, and (3) were flooded during the simulation.

Error	Ike		Matthew		Harvey		Florence	
	Coarse	*Mixed*	*Coarse*	*Mixed*	*Coarse*	*Mixed*	*Coarse*	*Mixed*
Stations	866,365	1,084,699	1,981,764	2,664,921	696,610	905,880	182,289	264,812
Best-Fit Slope	0.75	0.97	0.99	1.0	0.84	0.99	0.95	1.0
R^2	0.95	0.99	0.91	0.96	0.81	0.94	0.86	0.90
E_{RMS} (m)	0.72	0.14	0.22	0.13	0.24	0.12	0.22	0.18
B_{MN}	−0.28	−0.03	−0.01	0	−0.16	−0.01	−0.05	0

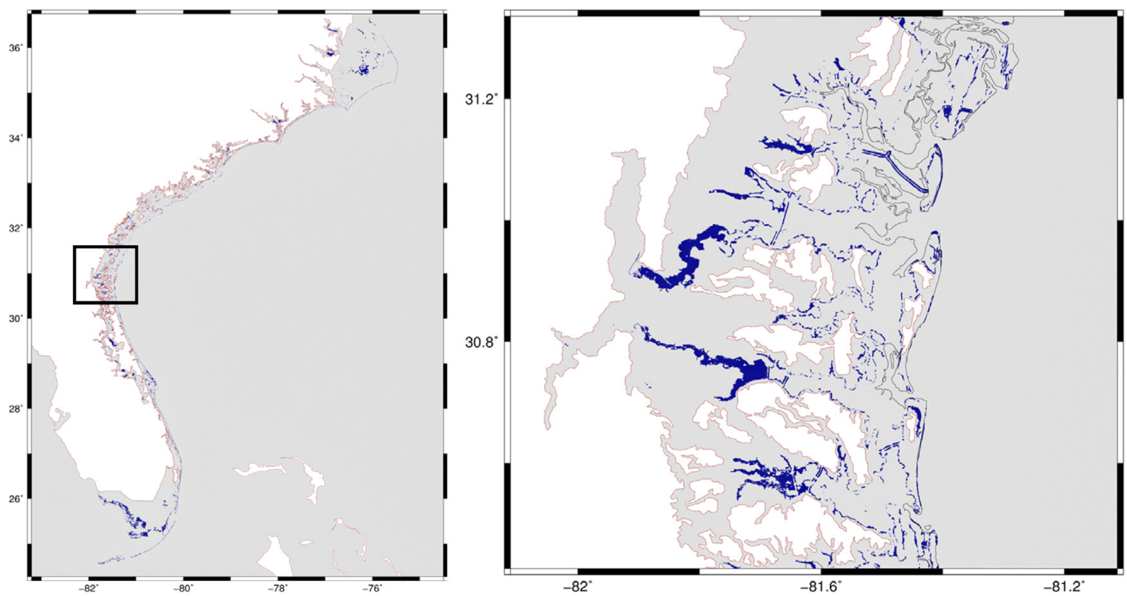

Fig. 5. Effect of mesh resolution on inland flooding predictions. Dark blue regions indicate locations where the *Coarse* results were dry and *Mixed* results were wet during Matthew. Black box indicates specific region as shown on the right. The fine-mesh boundary is shown in brown, and the black line in the right figure indicates the coastline.

(closer to unity) are also better. But the most interesting difference lies in the number of fine-mesh vertices that were used for comparison. The *Mixed* simulations have comparisons made at much higher numbers of vertices (about 218k more vertices for Ike, 680k for Matthew, 209k for Harvey, and 82k for Florence), indicating much more overland flooding as compared to the *Coarse* simulation.

This considerably larger number of comparison-points during Matthew is due to the larger region of analysis (FL to NC), as compared to individual states for other storms. Matthew was a shore-parallel storm that had effects from FL to NC (Fig. 2, second row, left column). The advantage of using the *Mixed* approach is evident at points that were dry during the *Coarse* simulation but were wetted in the *Mixed* simulation (Fig. 5). These additional wetted vertices are located along the wetting–drying regions like barrier islands, sounds, as well as upstream rivers, where the coarse mesh does not have sufficient resolution.

These trends in the difference in flooding extent between the *Coarse* and *Mixed* simulations are supported by the total volume of inundation (Table 3). For all storms, the *Mixed* and *Fine* simulations have comparable values, thus proving the effectiveness of the approach in matching the *Fine* simulation flooding extent. The *Coarse* simulation on the other hand, has a much lesser total volume as it floods lesser number of elements and lacks the flooding extents of both the *Mixed* and *Fine* simulations. The total volume of inundation for the *Coarse* simulation was less than that for the corresponding *Fine* simulation by 4.17×10^9 m^3 for Ike, 1.61×10^9 m^3 for Matthew, 0.58×10^9 m^3 for Harvey, and 0.66×10^9 m^3 for Florence. However, the total volume of inundation for the *Fine* simulation exceeded the value for the corresponding *Mixed* simulation by only 0.73×10^9 m^3 for Ike, 0.06×10^9 m^3 for Matthew, 0.15×10^9 m^3 for Harvey, and 0.04×10^9 m^3 for Florence.

Table 3
Predicted inundation volumes (10^9 m^3) for the *Coarse*, *Mixed*, and *Fine* simulations for all four storms. The results were mapped onto the fine mesh, and then inundation volumes were included for elements that (1) had ground surface elevations above mean sea level, (2) were located in the affected area of the storm, and (3) were flooded during the simulation.

Storm	Inundation volume (10^9 m^3)		
	Coarse	*Mixed*	*Fine*
Ike	5.63	9.07	9.80
Matthew	3.66	5.21	5.27
Harvey	0.33	0.76	0.91
Florence	0.98	1.60	1.64

The difference in the volume of inundation between the *Mixed* and *Fine* simulations is due to how the coastal region is represented in the coarse-mesh segment of the *Mixed* simulation. On the fine mesh, the peak surge during Ike was higher than 5 m along the Texas coastline east of Galveston Bay (Fig. 2, top row, left column) as this location experienced high shore-parallel winds at the time of landfall and afterward. This high peak-surge led to the largest volume of inundation compared to the other three storms (Table 3). But even for this high surge, the volume of inundation from the *Mixed* and *Fine* simulations differed by only 0.73×10^9 m^3. The corresponding difference between the *Coarse* and *Fine* simulations was 4.17×10^9 m^3. Thus compared to the *Coarse* results, the *Mixed* approach allows for a more accurate flooding, as well as a much larger flooding extent, which can be crucial during forecasting.

Table 4
Comparison in simulation wall-clock times between the *Mixed* and *Fine* simulations. All simulations were completed on the Stampede2 computing cluster at the Texas Advanced Computing Center, on a total of 532 cores (including 10 writer cores). Each component simulation was run three times, and the minimum wall-clock times are reported.

Storm	Wall-clock time (min)					Change (%)
	Mixed				*Fine*	
	Coarse	Adcirpolate	Fine	Total		
Ike	39	8	35	82	102	−19.6
Matthew	29	12	202	243	393	−38.2
Harvey	20	8	71	99	103	−3.9
Florence	37	12	129	178	380	−53.2

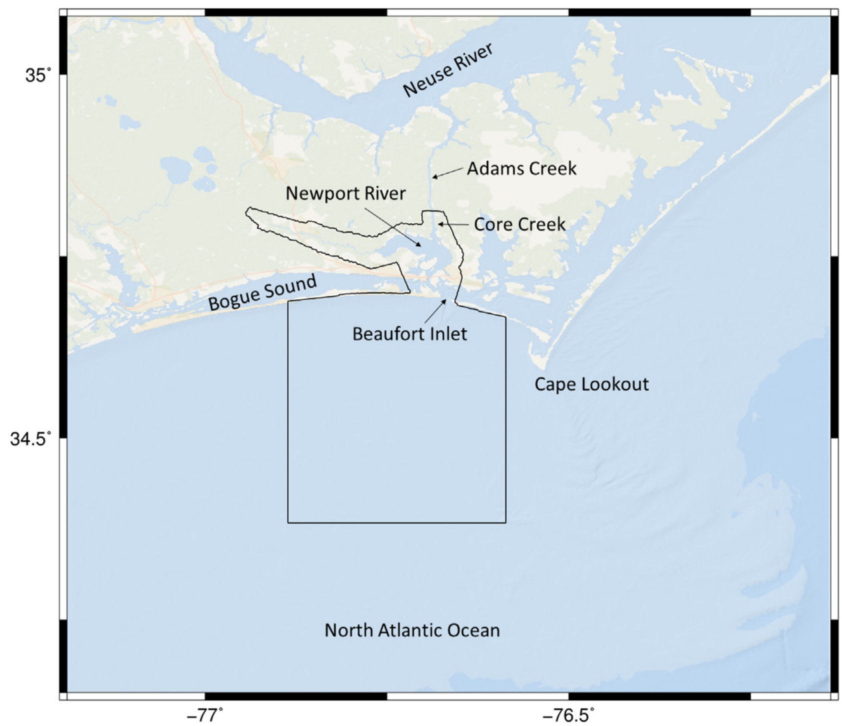

Fig. 6. Location of the *Adcirpolate* test-case domain in coastal North Carolina, including prominent geographic features.

3.2. Efficiency benefits

For all four storms, the total wall-clock time required for the *Mixed* simulation is compared with that for the corresponding *Fine* simulation (Table 4). There is a wide variety in the wall-clock times, depending on the size of each mesh (by total number of vertices/elements) and the number of simulation days on each mesh. For Ike and Harvey, the *Fine* simulations required 102 to 103 min, which was reduced by 3 to 19 percent with the *Mixed* simulations. For Matthew and Florence, the *Fine* simulations required 380 to 393 min, which was reduced by 38 to 53 percent in the *Fine* simulations. *Adcirpolate* required 8 to 12 min, or less than 10 percent of each *Mixed* simulation.

The multi-resolution approach had its maximum efficiency during Florence, with a run-time decrease of 53 percent. This efficiency is due to Florence's shore-normal track, which allowed switching after 6 days of simulation, when the storm first affected the NC coast. Thus the coarse mesh was used for most of the *Mixed* simulation, resulting in a lesser run time. There was also a large gain in efficiency during Matthew, with a run-time decrease of 38 percent. Because Matthew had a shore-parallel track, it affected a larger geographical extent for several days, and thus it required the fine mesh to be used for more of its *Mixed* simulation.

The relative sizes of the coarse and fine meshes (by number of vertices/elements) also affected the efficiency of the approach. For storms on the Atlantic coast, the fine FEMA-SAB mesh is more than three times larger than the coarse HSOFS mesh, whereas for storms on the Texas coast, the fine Texas mesh is about 1.8 times larger than the coarse HSOFS mesh. Because of this, there is a smaller potential for efficiency gains for storms on the Texas coast. For example during Harvey, the *Mixed* approach required 99 min, compared to the *Fine* simulation that required 103 min. Thus the run-time decrease was only 4 percent. But overall, the multi-resolution approach does have an efficiency gain for all storms, which is crucial especially in forecasting applications, because it can enable ensemble simulations to account for uncertainties in storm parameters.

4. Conclusions

High-fidelity predictions of coastal flooding require high resolution of small-scale flow pathways and barriers in coastal regions; this high resolution can be computationally costly. A multi-resolution approach was implemented in the ADCIRC modeling system. This approach allows the use of high-resolution meshes only when it is required, and without re-starting the simulation from scratch. The approach was evaluated for simulations of four storms that affected the U.S. coast

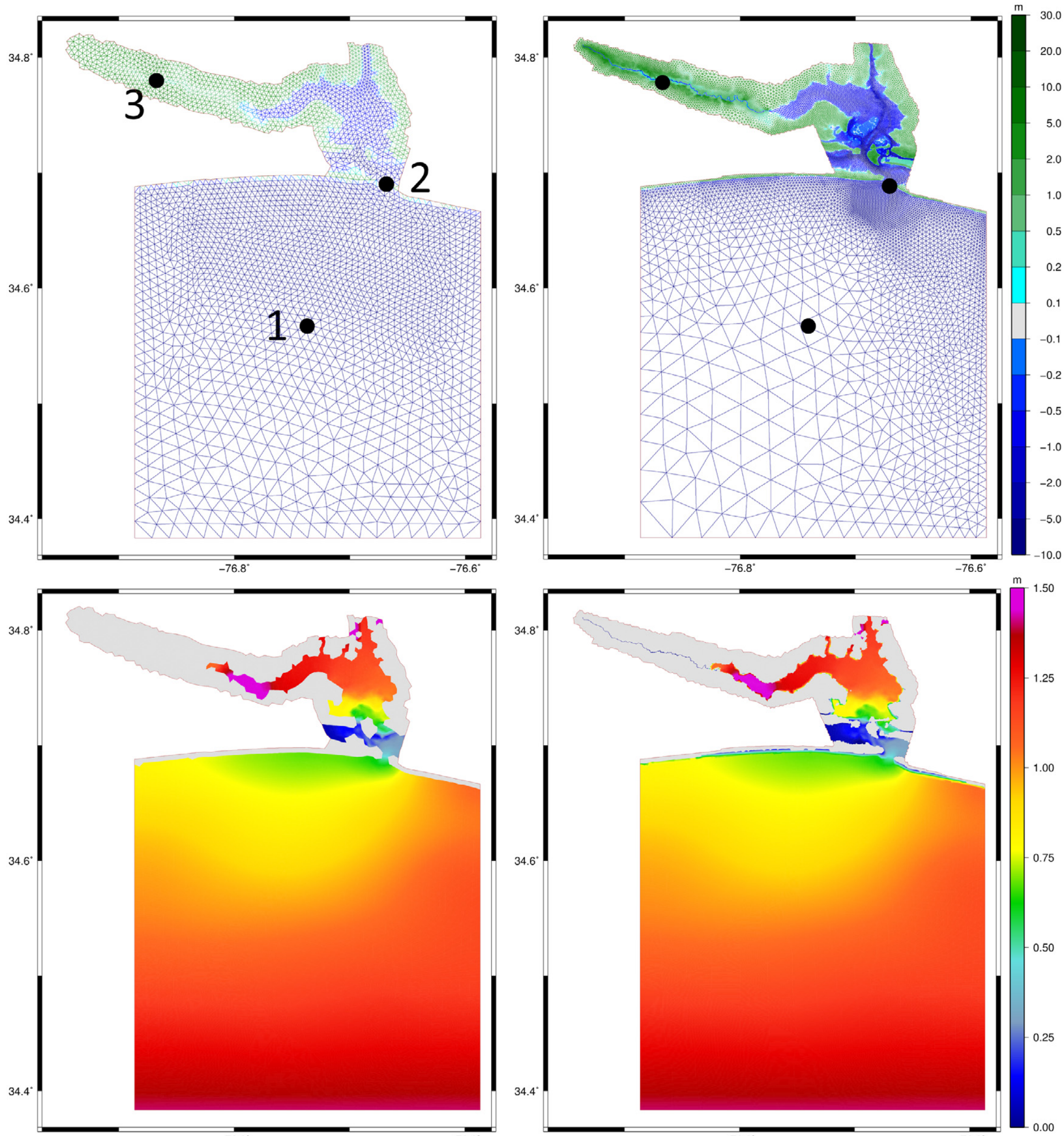

Fig. 7. Panels showing (top row) bathymetry (m) and (bottom row) water levels (m) from the *Mixed* simulation on the example case. Columns correspond to: (left) coarse mesh; and (right) fine mesh. The water levels shown are for: (bottom-left) at the end of the coarse part of *Mixed* before the switch, and (bottom-right) at the beginning of the fine part of *Mixed* after the switch. The water levels in (bottom-left) are interpolated/extrapolated to become the water levels in (bottom-right). Black dots indicate stations where water levels are shown in Fig. 8, and triangles indicate mesh elements.

in different regions. The benefits of the approach were evaluated in terms of accuracy and efficiency by comparisons to single simulations on coarse- and fine-resolution meshes. The major findings of this study are:

1. *If the simulation is switched at an acceptable time during the storm, then the flooding predictions will be similar to a full simulation on the higher-resolution mesh.* For all storms, the *Mixed* flooding predictions were similar to the *Fine* flooding predictions. However, they allowed flooding of a larger region as compared to the corresponding *Coarse* simulation. This extra flooding coverage was at regions like barrier islands and upstream rivers, where the coarse mesh did not have sufficient resolution to provide the required hydraulic connectivity for flooding to occur. At inland stations, the water levels reacted quickly to the switch onto the fine mesh.
2. *The multi-resolution approach can preserve the accuracy of high-resolution predictions of coastal flooding.* For all for storms, the *Mixed* results had a comparable accuracy to the *Fine* results. The R^2 and best-fit slopes were close to unity, the E_{RMS} values were less than 0.18 m, and the B_{MN} values were close to zero.
3. *The multi-resolution approach can enhance significantly the efficiency of high-resolution predictions of coastal flooding.* The *Mixed* simulations were more efficient than the *Fine* simulations. As measured by wall-clock times, the efficiency gains were between 3 to 53 percent, depending on the relative sizes and simulation durations on the meshes. *Adcirpolate* required less than 10 percent of the overall wall-clock time.

The multi-resolution approach is most promising for forecasting applications, in which the efficiency gains can translate directly into

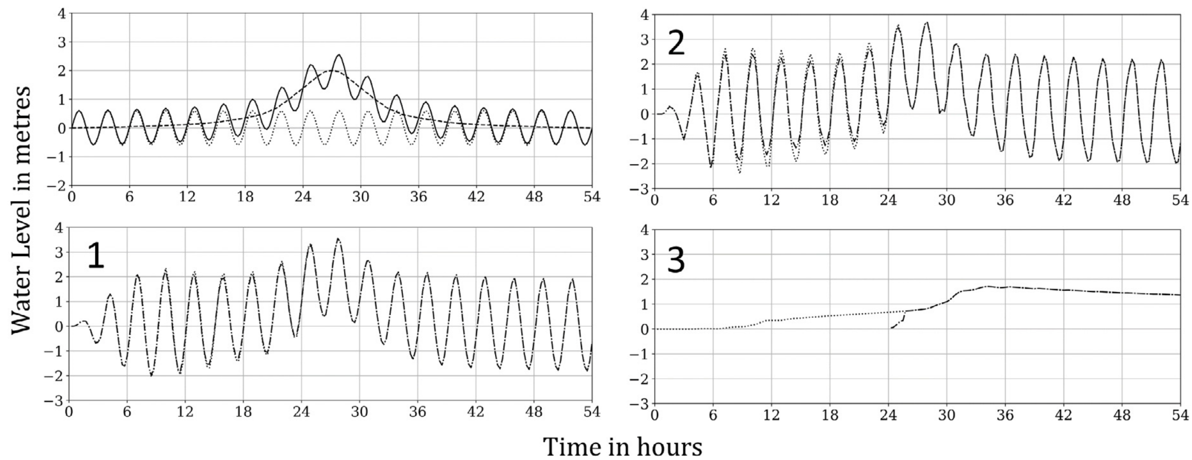

Fig. 8. Boundary forcing (m) and water levels (m) for the simple example. On the top-left is the variation in input forcing with line types corresponding to (dotted) tides-only, (dashed) surge-only, and (solid) tides plus surge. The other three plots indicate time-series of water levels (m) at the three stations shown in Fig. 7 with line types corresponding to: (dotted) *Fine*, and (dashed–dotted) *Mixed*.

additional time for decision-making. Future work will explore which conditions (coastal water levels, wind speeds, etc.) can be used to trigger the switch, and what is an optimal balance between accuracy losses and efficiency gains.

CRediT authorship contribution statement

Ajimon Thomas: Validation, Visualization, Writing - original draft. **J.C. Dietrich:** Supervision, Project administration, Writing - review & editing. **M. Loveland:** Investigation, Validation. **A. Samii:** Data curation, Methodology, Software. **C.N. Dawson:** Conceptualization, Funding acquisition, Software.

Declaration of competing interest

The authors declare that they have no known competing financial interests or personal relationships that could have appeared to influence the work reported in this paper.

Acknowledgments

This material is based upon work supported by the U.S. Department of Homeland Security under Grant Award Number 2015-ST-061-ND0001-01. The views and conclusions contained in this document are those of the authors and should not be interpreted as necessarily representing the official policies, either expressed or implied, of the U.S. Department of Homeland Security. This work was also supported by the National Science Foundation, United States of America grant ENH-1635784.

Appendix. Example of *Adcirpolate* in coastal North Carolina

To illustrate how *Adcirpolate* can be used to switch meshes during a simulation, we provide a small example for coastal North Carolina (Fig. 6). Beaufort Inlet is a barrier-island inlet located west of Cape Lookout, and leads south to the Atlantic Ocean. The domain also includes the tidal Newport River that flows into the Bogue Sound, and Core Creek that connects to Adams Creek, a tributary of the Neuse River. Due to the switching with *Adcirpolate* onto a higher-resolution mesh, the simulation will better represent the flow of surge farther up the Newport River.

Meshes with coarse and fine resolution were created by cutting the region from the HSOFS and SAB meshes, by using the Surface-water Modeling System (SMS, https://www.aquaveo.com/software/sms-surface-water-modeling-system-introduction). The coarse mesh has 3277 vertices with resolution varying from 1377 m at the ocean boundary on the south of the domain, to about 550 m at the inlet, to 315 m along the Core Creek, and to 350 m at the west end-point of the Newport River. The fine mesh has 22,375 vertices with element spacing varying from 888 to 2500 m at the ocean boundary, to 120 m at the inlet, to 85 m along the Core Creek, and to 25 m at the west end-point of the Newport River. The difference in resolution causes features to be represented differently between the two meshes (Fig. 7). The bathymetry of the Newport River extends about 20 km farther west in the fine mesh. The coarse mesh has 2 to 3 elements across the width of the Beaufort Inlet, compared to 10 elements in the fine mesh.

A tidal signal of period 3 hr and amplitude 1.2 m was added to a surge signal of peak amplitude 2 m, and applied as forcing (Fig. 8, top-left) on the bottom/south boundary of the two meshes. The total duration was 54 hr. The simulation started on the coarse mesh, but after 24 hr, when the water level on the ocean boundary reached 1.4 m, it was switched to the fine mesh for the remainder of the run. Before switching, at the end of the simulation on the coarse mesh (Fig. 7, bottom-left), the water levels were 1.4 m at the open coast, 0.35 to 0.5 m in the inlet, and 1 m at the west boundary of the Newport River. After switching, at the start of the simulation on the fine mesh (Fig. 7, bottom-right), these water levels were mapped to the true coastline, inlet and sound, and extended into the Newport River.

Water levels were analyzed at three stations: (1) open coast, (2) inlet, and (3) channel (with locations in Fig. 7), and for the *Fine* and *Mixed* simulations. At the open coast (station 1), there was no difference between the simulations, because both meshes had a sufficient resolution in open water to represent the combined tide and surge forcing. At the inlet (station 2), there are differences between the *Mixed* and *Fine* water levels before switching, due to differences in geometry between the coarse and fine meshes. But after switching, the water levels match exactly. At the channel (station 3), the *Mixed* simulation stays dry for the first 24 hr, because the coarse mesh does not have sufficient resolution to represent the fine channel. However, very shortly after the switch, the water levels in *Mixed* increased to match the *Fine* results. This was an increase of 0.75 m in just a couple of hours, with no oscillations or instabilities in the computed solution. Thus, even when the coarse mesh had locations that were dry, the *Mixed* simulation was able to 'catch up' to the *Fine* results.

References

Altuntas, A., Baugh, J., 2017. Adaptive subdomain modeling: A multi-analysis technique for ocean circulation models. Ocean Model. 115, 86–104.

Baugh, J., Altuntas, A., Dyer, T., Simon, J., 2015. An exact reanalysis technique for storm surge and tides in a geographic region of interest. Coast. Eng. 97, 60–77.

Behrens, J., Bader, M., 2009. Efficiency considerations in triangular adaptive mesh refinement. Phil. Trans. R. Soc. A Math. Phys. Eng. Sci. 367, 4577—4589.

Behrens, J., Rakowsky, N., Hiller, W., Handorf, D., Lauter, M., Papke, J., Dethloff, K., 2005. Amatos: Parallel adaptive mesh generator for atmospheric and oceanic simulation. Ocean Model. 10, 171–183.

Beisiegel, N., Vater, S., Behrens, J., Dias, F., 2020. An adaptive discontinuous Galerkin method for the simulation of hurricane storm surge. Ocean Dyn. 70, 641–666.

Berg, R., 2009. Tropical Cyclone Report, Hurricane Ike, 1-14 September 2008. Tech. rep., National Hurricane Center.

Berger, M.J., George, D.L., Leveque, R.J., Mandli, K.T., 2011. The GeoClaw software for depth-averaged flows with adaptive refinement. Adv. Water Resour. 34, 1195–1206.

Bhaskaran, P.K., Nayak, S., Bonthu, S.R., Murthy, P.L.N., Sen, D., 2013. Performance and validation of a coupled parallel ADCIRC-SWAN model for THANE cyclone in the Bay of Bengal. Environ. Fluid Mech. 13, 601–623.

Bilskie, M.V., Hagen, S.C., Medeiros, S.C., 2020. Unstructured finite element mesh decimation for real-time Hurricane storm surge forecasting. Coast. Eng. 156, 103622.

Bunya, S., Dietrich, J.C., Westerink, J.J., Ebersole, B.A., Smith, J.M., Atkinson, J.H., Jensen, R.E., Resio, D.T., Luettich, R.A., Dawson, C.N., Cardone, V.J., Cox, A.T., Powell, M.D., Westerink, H.J., Roberts, H.J., 2010. A high-resolution coupled riverine flow, tide, wind, wind wave and storm surge model for southern Louisiana and Mississippi: Part I – Model development and validation. Mon. Weather Rev. 138, 345–377.

Cardone, V.J., Cox, A.T., 2009. Tropical cyclone wind field forcing for surge models: Critical issues and sensitivities. Nat. Hazards 51, 29–47.

Caviedes-Voulliéme, D., Gerhard, N., Sikstel, A., M uller, S., 2020. Multiwavelet-based mesh adaptivity with discontinuous Galerkin schemes: Exploring 2D shallow water problems. Adv. Water Resour. 138, 103559.

Cheung, K.F., Phadke, A.C., Wei, Y., Rojas, R., Douyere, Y.J.M., Martino, C.D., Houston, S.H., Liu, P.L.F., Lynett, P.J., Dodd, N., Liao, S., Nakazaki, E., 2003. Modeling of storm-induced coastal flooding for emergency management. Ocean Eng. 30, 1353–1386.

Conner, W.C., Kraft, R.H., Harris, D.L., 1957. Empirical methods for forecasting the maximum storm tide due to hurricanes and other tropical storms. Mon. Weather Rev. 85, 113–116.

Corbosiero, K.L., Wng, Chen, Y., Dudhia, J., Davis, C., 2007. Advanced research WRF high frequency model simulations of the inner core structures of hurricanes katrina and rita (2005). In: Proceedings from the Eighth WRF User's Workshop. National Center for Atmospheric Research, Boulder, CO.

Cox, A.T., Greenwood, J.A., Cardone, V.J., Swail, V.R., 1995. An interactive objective kinematic analysis system. In: C.N. Dawson and M. Gerritsen (Eds.), Proceedings of the Fourth International Workshop on Wave Hindcasting and Forecasting. pp. 109–118.

Debreu, L., Marchesiello, P., Penven, P., Cambon, G., 2012. Two-way nesting in split-explicit ocean models: algorithms, implementation and validation. Ocean Model. 49–50, 1–21.

Debreu, L., et al., 2008. AGRIF: Adaptive grid refinement in fortran. Comput. Geosci. 34, 8–13.

Dietrich, J.C., Bunya, S., Westerink, J.J., Ebersole, B.A., Smith, J.M., Atkinson, J.H., Jensen, R.E., Resio, D.T., Luettich, R.A., Dawson, C.N., Cardone, V.J., Cox, A.T., Powell, M.D., Westerink, H.J., Roberts, H.J., 2010. A high-resolution coupled riverine flow, tide, wind, wind wave and storm surge model for southern Louisiana and Mississippi: Part II – Synoptic description and analysis of hurricanes katrina and rita. Mon. Weather Rev. 138, 378–404.

Dietrich, J.C., Muhammad, A., Curcic, M., Fathi, A., Dawson, C.N., Chen, S.S., Luettich, R.A., 2018. Sensitivity of storm surge predictions to atmospheric forcing during hurricane isaac. J. Waterw. Port Coast. Ocean Eng. 144.

Dietrich, J.C., Tanaka, S., Westerink, J.J., Dawson, C.N., Luettich, R.A., Zijlema, M., Holthuijsen, L.H., Smith, J.M., Westerink, L.G., Westerink, H.J., 2012. Performance of the unstructured-mesh, SWAN+ADCIRC model in computing hurricane waves and surge. J. Sci. Comput. 52, 468–497.

Dietrich, J.C., Westerink, J.J., Kennedy, A.B., Smith, J.M., Jensen, R.E., Zijlema, M., Holthuijsen, L.H., Dawson, C.N., Luettich, R.A., Powell, M.D., Cardone, V.J., Cox, A.T., Stone, G.W., Pourtaheri, H., Hope, M.E., Tanaka, S., Westerink, L.G., Westerink, H.J., Cobell, Z., 2011. Hurricane gustav (2008) waves and storm surge: Hindcast, validation and synoptic analysis in southern Louisiana. Mon. Weather Rev. 139, 2488–2522.

Dinapoli, M.G., Simionato, C.G., Moreira, D., 2020. Development and validation of a storm surge forecasting/hindcasting modelling system for the extensive Rio de la Plata Estuary and its adjacent Continental Shelf. Nat. Hazards 103, 2231–2259.

Fauver, L.A., 1970. A Study of the Wind Field in the Planetary Boundary Layer of a Moving Tropical Cyclone (Master's thesis). School of Engineering and Science, New York University.

Federal Emergency Management Agency, 2019. Guidance for Flood Risk Analysis and Mapping: Determination of Wave Characteristics. Tech. rep..

FEMA, 2021. Flood risk study engineering library. https://hazards.fema.gov/wps/portal/frisel [Retrieved 4 February 2021].

Gao, J., Luettich, R.A., Fleming, J.G., 2017. Development and evaluation of a generalized asymmetric tropical cyclone vortex model in ADCIRC.

Garratt, J.R., 1977. Review of drag coefficients over oceans and continents. Mon. Weather Rev. 105, 915–929.

Gerhard, N., Caviedes-Voulliéme, D., M uller, S., Kesserwani, G., 2015. Multiwavelet-based grid adaptation with discontinuous Galerkin schemes for shallow water equations. J. Comput. Phys. 301, 265–288.

Hill, C., DeLuca, C., Balaji, V., Suarez, M., da Silva, A., 2004. Architecture of the earth system modeling framework. Comput. Sci. Eng. 6.

Holland, R.W., 1980. An analytic model of the wind and pressure profiles in hurricanes. Mon. Weather Rev. 108, 1212–1218.

Hope, M.E., Westerink, J.J., Kennedy, A.B., Kerr, P.C., Dietrich, J.C., Dawson, C.N., Bender, C.J., Smith, J.M., Jensen, R.E., Zijlema, M., Holthuijsen, L.H., Luettich Jr, R.A., Powell, M.D., Cardone, V.J., Cox, A.T., Pourtaheri, H., Roberts, H.J., Atkinson, J.H., Tanaka, S., Westerink, H.J., Westerink, L.G., 2013. Hindcast and validation of hurricane ike (2008) waves, forerunner, and storm surge. J. Geophys. Res.: Oceans 118, 4424–4460.

Hou, J., Wang, R., Liang, Q., Li, Z., Huang, M.S., Hinkelmann, R., 2018. Efficient surface water flow simulation on static Cartesian grid with local refinement according to key topographic features. Comput. Fluids 176, 117—134.

Hovermale, J.B., 1976. The Movable Fine Mesh (MFM)-A New Operational Forecast Model. Tech. rep., National Weather Service.

Hu, R., Fang, F., Salinas, P., Pain, C.C., 2018. Unstructured mesh adaptivity for urban flooding modelling. J. Hydrol. 560, 354–363.

Interagency Performance Evaluation Task Force, 2008. Performance Evaluation of the New Orleans and Southeast Louisiana Hurricane Protection System. Tech. rep., US Army Corps of Engineers.

Kennedy, A.B., Gravois, U., Zachry, B.C., Westerink, J.J., Hope, M.E., Dietrich, J.C., Powell, M.D., Cox, A.T., Luettich, R.A., Dean, R.G., 2011. Origin of the hurricane ike forerunner surge. Geophys. Res. Lett. 38 (8).

Kesserwani, G., Liang, Q., 2012. Dynamically adaptive grid based discontinuous Galerkin shallow water model. Adv. Water Resour. 37, 23–39.

Kubatko, E.J., Westerink, J.J., Dawson, C.N., 2006. Hp discontinuous Galerkin methods for advection dominated problems in shallow water flow. Comput. Methods Appl. Mech. Engrg. 196, 437–451.

Liang, Q., Hou, J., Xia, X., 2015. Contradiction between the c-property and mass conservation in adaptive grid based shallow flow models: cause and solution. Internat. J. Numer. Methods Fluids 78, 17–36.

Liang, Q., Marche, F., 2009. Numerical resolution of well-balanced shallow water equations with complex source terms. Adv. Water Resour. 32, 873–884.

Luettich, R.A., Westerink, J.J., 2004. Formulation and Numerical Implementation of the 2D/3D ADCIRC Finite Element Model Version 44.XX. University of North Carolina at Chapel Hill, https://adcirc.org/files/2018/11/adcirc_theory_2004_12_08.pdf.

Luettich, R.A., Westerink, J.J., Scheffner, N.W., 1992. ADCIRC: An Advanced Three-Dimensional Circulation Model for Shelves Coasts and Estuaries, Report 1: Theory and Methodology of ADCIRC-2DDI and ADCIRC- 3DL. Tech. rep., United States Army Corps of Engineers.

Mandli, K.T., Dawson, C.N., 2014. Adaptive mesh refinement for storm surge. Ocean Model. 75, 36–50.

Mathur, M.B., 1974. A multiple-grid primitive equation model to simualte the development of an asymmetric hurricane (Isbell,1964). J. Atmos. Sci. 31, 371–393.

Miyakoda, K., Rosati, A., 1977. One-way nested grid models: The interface conditions and the numerical accuracy. Mon. Weather Rev. 105, 1092–1107.

Myers, E., Hess, K., Yang, Z., Xu, J., Wong, A., Doyle, D., Woolard, J., White, S., Le, B., Gill, S., Hovis, G., 2007. VDatum and strategies for national coverage. In: Proceedings of the IEEE OCEANS Conference.

National Oceanic, Atmospheric Administration, 2021. Storm surge and tide operational forecast. https://polar.ncep.noaa.gov/estofs/ [Retrieved 1 March 2021].

Oey, L.Y., Chen, P., 1992. A nested-grid ocean model: With application to the simulation of meanders and eddies in the Norvegian coastal current. J. Geophys. Res. 97, 20063–20086.

Ookochi, Y., 1972. A computational scheme of the nesting fine mesh in the primitive equation model. Japan Meteorol. Agency 50, 37–48.

Penven, P., et al., 2006. Evaluation and application of the ROMS 1-way embedding procedure to the central California upwelling system. Ocean Model. 12, 157–187.

Pianezze, J., Barthe, C., Bielli, S., Tulet, P., Jullien, S., Cambon, G., Bousquet, O., Claeys, M., Cordier, E., 2020. A new coupled ocean-waves-atmosphere model designed for tropical storm studies: Example of tropical cyclone bejisa (2013-2014) in the South-West Indian ocean. J. Adv. Modelling Earth Syst. 10, 801–825.

Powell, M.D., Houston, S.H., Reinhold, T.A., 1996. Hurricane andrew's landfall in south florida, part I: Standardizing measurements for documentation of surface wind fields. Weather Forecast. 11, 304–328.

Powell, M.D., Murillo, S., Dodge, P., Uhlhorn, E., Gamache, J., Cardone, V., Cox, A., Otero, S., Carrasco, N., Annane, B., Fleur, R.S., 2010. Reconstruction of hurricane katrina's wind fields for storm surge and wave hindcasting. Ocean Eng. 37, 26–36.

Riverside Technology, AECOM, 2015. Mesh Development, Tidal Validation, and Hindcast Skill Assessment of an ADCIRC Model for the Hurricane Storm Surge Operational Forecast System on the US Gulf-Atlantic Coast. Tech. rep..

Roberts, K.J., Dietrich, J.C., Wirasaet, D., Pringle, W.J., Westerink, J.J., 2021. Dynamic load balancing for predictions of storm surge and coastal flooding. Environ. Model. Softw. (in re-review).

Roberts, K.J., Pringle, W.J., Westerink, J.J., 2019. On the automatic and a priori design of unstructured mesh resolution for coastal ocean circulation models. Ocean Model. 144, 101509.

Samii, A., 2021. Adcirpolate: A toolset for interpolating data between different ADCIRC meshes. https://github.com/ccht-ncsu/Adcirpolate, Accessed 15 Mar 2021.

Sebastian, A.G., Proft, J.M., Dietrich, J.C., Du, W., Bedient, P.B., Dawson, C.N., 2014. Characterizing hurricane storm surge behavior in galveston bay using the SWAN+ADCIRC model. Coast. Eng. 88, 171–181.

Stewart, S.R., 2017. Tropical Cyclone Report for Hurricane Matthew, 28 September - 9 October 2016. Tech. rep., National Hurricane Center.

Stewart, S.R., Berg, R., 2019. Tropical Cyclone Report for Hurricane Florence, 31 August – 17 September 2018. Tech. rep., National Hurricane Center.

Suh, S.W., Lee, H.Y., Kim, H.J., Fleming, J.G., 2015. An efficient early warning system for typhoon storm surge based on time-varying advisories by coupled ADCIRC and SWAN. Ocean Dyn. 65, 617–646.

Taeb, P., Weaver, R.J., 2019. An operational coastal forecasting tool for performing ensemble modeling. Estuar. Coast. Shelf Sci. 217, 237–249.

Tanaka, S., Bunya, S., Westerink, J.J., Dawson, C.N., Luettich, R.A., 2011. Scalability of an unstructured grid continuous Galerkin based hurricane storm surge model. J. Sci. Comput. 46, 329–358.

Thomas, A., 2020. Using a Multi-Resolution Approach to Improve the Accuracy and Efficiency of Flooding Predictions (Ph.D. thesis). North Carolina State University, Raleigh, NC, USA.

Thomas, A., Dietrich, J.C., Asher, T.G., Blanton, B.O., Cox, A.T., Dawson, C.N., Fleming, J.G., Luettich, R.A., 2019. Influence of storm timing and forward speed on tide-surge interactions during hurricane matthew. Ocean Model. 137, 1–19. http://dx.doi.org/10.1016/j.ocemod.2019.03.004.

U.S. Army Corps of Engineers, 2018. North atlantic coast comprehensive study report. http://www.nad.usace.army.mil/CompStudy/ [Retrieved 13 March 2018].

Vickery, P.J., Skerlj, P.F., Steckley, A.C., Twisdale, L.A., 2000. Hurricane wind field model for use in hurricane simulations. J. Struct. Eng. 126, 1203–1221.

Westerink, J.J., Luettich Jr, R.A., Feyen, J.C., Atkinson, J.H., Dawson, C.N., Roberts, H.J., Powell, M.D., Dunion, J.P., Kubatko, E.J., Pourtaheri, H., 2008. A basin to channel scale unstructured grid hurricane storm surge model applied to southern Louisiana. Mon. Weather Rev. 136, 833–864.